JOURNAL OF COMPUTATIONAL PHYSICS **132,** 374–383 (1997)
ARTICLE NO. CP965645

Efficient Algorithm for Solving Inverse Source Problems of a Nonlinear Diffusion Equation in Microwave Heating

X. Chen* and Y. M. Chen†

*Department of Applied Mathematics and Statistics, State University of New York, Stony Brook, New York 11794; †Numerical Computation Corporation, 57 Quaker Path, Stony Brook, New York 11790

Received February 29, 1996; revised August 19, 1996

Determination of the equivalent internal heat source from surface temperature measurements in microwave processing of materials is formulated as an inverse source problem of a nonlinear diffusion equation. The versatile generalized pulse-spectrum technique (GPST) inversion algorithm with the incorporation of multi-level grid method and hierarchical parallelism is developed for solving this type of inverse problems. Development of a simple 2D code has been completed. Numerical simulations are carried out to test the feasibility and capability of this improved GPST without the real measurement data. It is found that this new inversion algorithm not only does produce very good results but also is much more efficient and stable than its standard version.

INTRODUCTION

Microwave heating is used generally for changing material characteristics, separating and bonding different materials, and processing a wide variety of ceramic materials. As a matter of fact, microwave processing of ceramics is one of the most important modern industrial processes [18, 16, 1]. In microwave processing, high thermal stresses often cause the undesirable cracking of samples. Hence knowledge of temperature distribution in the sample is crucial in overcoming this type of problems. The entire physical phenomenon of microwave heating can be described by the solution of the initial-boundary value problem of the Maxwell's equations coupled with a nonlinear diffusion equation, but this system of seven partial differential equations is just too costly to solve in general. Here we propose to simplify this problem by first representing the effects of the microwave energy loss in the sample with an unknown equivalent internal heat source and then solving an inverse source problem of the nonlinear diffusion equation from the surface temperature to determine this unknown internal heat source. These surface temperature data can be obtained by using the independent infrared sensors. In other words, what we are proposing here is that one solves an inverse source problem of one PDE in a much smaller domain (including the sample only), instead of the original initial-boundary value problem of seven PDEs in a much larger domain (inclusing both sample and microwave oven). The advantage in computation can be illustrated by a simple comparison of the computational efforts of these two approaches. Based on an implicit 3D finite difference scheme and Gaussian elimination solver for matrices, a rough estimate of the asymptotic number of floating point arithmetic operations (FLO) count for the initial-boundary value problem of seven PDEs is $\mathrm{FLO}_{\mathrm{di}} = \mathrm{O}(mTYB^2/2)$, where $m = 7$ is the number of PDEs, $T = \mathrm{O}(10^2)$ is the number of time steps needed in simulation, $Y = \mathrm{O}(y^3)$ is the total number of grid points for the microwave oven containing the sample, y is the number of grid points in one direction, $B = \mathrm{O}(mY^{2/3})$ is the bandwidth of the matrix. Hence $\mathrm{FLO}_{\mathrm{di}} = \mathrm{O}(1.7 \times 10^4 y^7)$. Similarly, based on the standard generalized pulse-spectrum technique (GPST) without any refinement [5], the asymptotic FLO count for the inverse source problem of one PDE is $\mathrm{FLO}_{\mathrm{inv}} = \mathrm{O}(Nk^3Z^3/3)$, where $k = 3$ is the number of unknown parameters of heat source, $N = \mathrm{O}(10)$ is the number of iterations needed for the convergence of GPST, $Z = \mathrm{O}(z^3)$ is the total number of grid points for the sample only, z is the number of grid points in one direction. Hence $\mathrm{FLO}_{\mathrm{inv}} = \mathrm{O}(90z^9)$. The approximate condition for the preference of solivng the inverse source problem of one PDE than the initial-boundary value problem of a system of seven PDEs is $\mathrm{FLO}_{\mathrm{inv}} < \mathrm{FLO}_{\mathrm{di}}$; i.e., $z^9 < 188y^7$. In general, $y = \mathrm{O}(3z)$ and then the condition becomes $z < 641$ which is more than enough, for in practice, $z = \mathrm{O}(10^2)$.

Up to the present, very little research has been done for solving the inverse source problems of diffusion equations. On the other hand, much research has been done for solving the inverse coefficient problems of diffusion equations [4, 3, 6, 12, 11, 7, 14] and for the inverse boundary-condition problems of diffusion equations [2, 10]. Here the versatile GPST inversion algorithm [6, 7, 12, 13], with the novel incorporation of the multilevel grid method [8, 9, 20], and the hierarchical parallelism [5, 9] is developed for solving this type of inverse source problem. For simplicity, here only a 2D code based on the polar coordinate is developed. Due to the lack of access to multiprocessor computers, numerical simulations are carried out only on a single proc-

0021-9991/97 $25.00

essor computer to test the feasibility and capability of this improved GPST inversion algorithm without the real measurement data. It is found that this new inversion algorithm not only produces very good results, but also it is much more efficient and stable than its standard version, even on a single processor computer. We cannot compare our results with others, because through an extensive literature search we are not able to find any.

GOVERNING EQUATIONS AND MATHEMATICAL FORMULATION

The partial differential equations governing the microwave heating of ceramic materials are

$$\begin{aligned} &\nabla \times \nabla \times \mathbf{E} - \mu_0 \partial^2 \varepsilon(\mathbf{x}, T)\mathbf{E}/\partial t^2 + \mu_0 \partial \sigma(\mathbf{x}, T)\mathbf{E}/\partial t = 0, \\ &\mathbf{x} \in \Omega, 0 < t < \infty, \nabla \cdot [\kappa(\mathbf{x}, T)\nabla T] - C\rho(\mathbf{x}, T)\partial T/\partial t \\ &\quad + \sigma(\mathbf{x}, T)\mathbf{E} \cdot \mathbf{E}^*/2 = 0, \\ &\mathbf{x} \in \Omega_0 \subset \Omega, 0 < t < \infty, \end{aligned} \tag{1}$$

with the appropriate initial-boundary conditions for $\mathbf{E}(\mathbf{x}, t)$ on $\partial\Omega$ and $\partial\Omega_0$ and the convective-radiative boundary condition for $T(\mathbf{x}, t)$ [15]

$$\begin{aligned} \kappa(\mathbf{x}, T)\partial T/\partial \mathbf{n} &= h(T_r - T) + s(\alpha T_r^4 - \beta T^4), \\ \mathbf{x} &\in \partial\Omega_0, 0 < t < \infty, \end{aligned} \tag{2}$$

and the initial condition for T,

$$T(\mathbf{x}, 0) = T_r(\mathbf{x}), \quad \mathbf{x} \in \Omega_0 + \partial\Omega_0, \tag{3}$$

where Ω is the interior of a microwave oven with boundary $\partial\Omega$, Ω_0 is the ceramic sample with boundary $\partial\Omega_0$, $\partial \cdot/\partial \mathbf{n}$ is the derivative normal to $\partial\Omega_0$, $\mathbf{E}(\mathbf{x}, t)$ is the electric field, $T(\mathbf{x}, t)$ is the temperature distribution in the sample, μ_0 is the free space permeability, $\varepsilon(\mathbf{x}, T)$ is the permittivity, $\sigma(\mathbf{x}, T)$ is the conductivity, $\kappa(\mathbf{x}, T)$ is the thermal conductivity of the sample, the constant C is the specific heat of the sample, $\rho(\mathbf{x}, T)$ is the density of the sample, h is the convective unit surface conductance of the sample, s is the Stefan–Boltzman constant, and β and α are the emissivity of the surface of the sample and that of the free space, respectively.

Since the task of solving Eqs. (1)–(3) is either extremely difficult or impossible in general, here we propose to simplify the problem by first eliminating the Maxwell's equation in (1) and replacing the electromagnetic power dissipation term $\sigma\mathbf{E} \cdot \mathbf{E}^*/2$ in the nonlinear diffusion equation by an unknown equivalent internal heat source $Q(\mathbf{x}, T)$, i.e., Eq. (1) is replaced by

$$\begin{aligned} &\nabla \cdot [\kappa(\mathbf{x}, T)\nabla T] - C\rho(\mathbf{x}, \mathbf{T})\partial T/\partial t + Q(\mathbf{x}, T) = 0, \\ &\quad \mathbf{x} \in \Omega_0, 0 < t < \infty, \end{aligned} \tag{4}$$

where in the finite range of T (0 to 1400°C), $Q(\mathbf{x}, T)$ is a simple quadratic function of T [17] and can be approximated amply by the cubic polynomials,

$$Q(\mathbf{x}, T) = c_1(\mathbf{x})T + c_2(\mathbf{x})T^2 + c_3(\mathbf{x})T^3. \tag{5}$$

Next in addition to the process of microwave heating, the surface temperature of the sample is measured independently at few locations by infrared sensers to provide the auxiliary condition

$$\begin{aligned} T(\mathbf{x}_p, t_v) &= T_S(\mathbf{x}_p, t_v), \quad \mathbf{x}_p \in \partial\Omega_0; \\ p &= 1, 2, 3, ..., P; v = 1, 2, 3, ... \end{aligned} \tag{6}$$

Now, solving the initial-boundary value problem of Eqs. (1)–(3) is replaced by first solving the inverse source problem of Eqs. (2)–(6) to obtain the equivalent internal heat source Q and then solving the initial-boundary value problem of Eqs. (2)–(5) to obtain the temperature distribution of the sample.

GENERALIZED PULSE-SPECTRUM TECHNIQUE (GPST)

The GPST iterative inversion algorithm begins by setting

$$\begin{aligned} T_{n+1}(\mathbf{x}, t) &= T_n(\mathbf{x}, t) + \delta T_n(\mathbf{x}, t), \\ c_{l,n+1}(\mathbf{x}) &= \mathbf{c}_{l,n}(\mathbf{x}) + \delta c_{l,n}(\mathbf{x}), \\ l &= 1, 2, 3; n = 0, 1, 2, 3 ..., \end{aligned} \tag{7}$$

where for convergence the δ-terms are smaller than their corresponding non-δ-terms in some norms and the $c_{l,0}$'s are the initial guesses for the corresponding unknown c_l's.

Upon substituting (7) into Eqs. (2)–(5) and neglecting terms of $O(\delta^2)$ and higher, one obtains the same nonlinear diffusion equation for T_n as that for T, except with the additional subscript "n,"

$$\begin{aligned} &\nabla \cdot [\kappa_n \nabla T_n] - C\rho_n \partial T_n/\partial t + (c_{1,n}T_n + c_{2,n}T_n^2 + c_{3,n}T_n^3) = 0, \\ &\quad \mathbf{x} \in \Omega_0, 0 < t < \infty, n = 0, 1, 2, 3, ..., \end{aligned} \tag{8}$$

$$\begin{aligned} \kappa_n \partial T_n/\partial \mathbf{n} &= h(T_r - T_n) + s(\alpha T_r^4 - \beta T_n^4), \\ \mathbf{x} &\in \partial\Omega_0, 0 < t < \infty, \end{aligned} \tag{9}$$

and

$$T_n(\mathbf{x}, 0) = T_r(\mathbf{x}), \quad \mathbf{x} \in \Omega_0 + \partial\Omega_0, \tag{10}$$

where $\kappa_n \equiv \kappa(\mathbf{x}, T_n)$ and $\rho_n \equiv \rho(\mathbf{x}, T_n)$, and a linear diffusion equation for δT_n,

$$\nabla\cdot[\kappa_n\nabla\delta T_n]+\nabla\cdot(\delta T_n\nabla T_n\partial\kappa_n/\partial T_n)-C\rho_n\partial\delta T_n/\partial t$$
$$-C(\partial\rho_n/\partial T_n)(\partial T_n/\partial t)\delta T_n+(c_{1,n}+2c_{2,n}T_n+3c_{3,n}T_n^2)\delta T_n$$
$$=-T_n\delta c_{1,n}-T_n^2\delta c_{2,n}-T_n^3\delta c_{3,n},\ \mathbf{x}\in\Omega_0,$$
$$0<t<\infty, n=0,1,2,3,..., \tag{11}$$
$$\kappa_n\partial\delta T_n/\partial\mathbf{n}=-[h+4s\beta T_n^3+(\partial\kappa_n/\partial T_n)(\partial T_n/\partial\mathbf{n})]\delta T_n,$$
$$\mathbf{x}\in\partial\Omega_0, 0<t<\infty, \tag{12}$$

and

$$\delta T_n(\mathbf{x},0)=0,\quad \mathbf{x}\in\Omega_0+\partial\Omega_0. \tag{13}$$

By using the method of Green's function, the solution of Eqs. (11)–(13) can be expressed in the integral relation

$$\int_0^\infty\int_{\Omega_0} G_n(\mathbf{x},t;\mathbf{x}',t')(\delta c_{1,n}T_n+\delta c_{2,n}T_n^2+\delta c_{3,n}T_n^3)\,d\mathbf{x}'\,dt'$$
$$=T_n-T_{n+1}, n=0,1,2,3,..., \tag{14}$$

where $G_n(\mathbf{x}, t; \mathbf{x}', t')$ is the appropriate Green's function of Eqs. (11)–(13).

For speeding up the convergence and eliminating the unknown T_{n+1} in (14), one can first set $(\mathbf{x}, t)$ to $(\mathbf{x}_p, t_v)$, $p = 1, 2, 3, ..., P$; $v = 1, 2, 3, ..., \Upsilon$, where the surface temperature T_S is measured at the pth location and the vth time step, and then replace $T_{n+1}(\mathbf{x}_p, t_v)$ by the measured temperature $T_S(\mathbf{x}_p, t_v)$. Hence the integral form (14) is reduced to a system of Fredholm integral equations of the first kind for the unknowns $\delta c_{1,n}$, $\delta c_{2,n}$, and $\delta c_{3,n}$,

$$\int_0^\infty\int_{\Omega_0} G_n(\mathbf{x}_p,t_v;\mathbf{x}',t')(\delta c_{1,n}T_n+\delta c_{2,n}T_n^2+\delta c_{3,n}T_n^3)\,d\mathbf{x}'\,dt'$$
$$=T_n(\mathbf{x}_p,t_v)-T_S(\mathbf{x}_p,t_v), p=1,2,3,...,P; \tag{15}$$
$$v=1,2,3,...,\Upsilon; n=0,1,2,3,....$$

Theoretically, Eqs. (7)–(10) and (15) form the basic structure of each GPST iteration. Each cycle of GPST iteration consists of a direct half-cycle in which (8)–(10) are solved and an inverse half-cycle in which (7) and (15) are solved. However, in practice it is extremely difficult to find the Green's function and then to solve the system of integral equations (15). On the other hand, one can first discretize (11)–(13) the same way as for (8)–(10) to obtain a linear algebraic relation, and then one utilizes the same method from above to transform the derived linear algebraic relation into a system of linear algebraic equations for the unknowns $\delta c_{1,n}$, $\delta c_{2,n}$, and $\delta c_{3,n}$.

On a uniform circular cylindrical grid with I increments of Δr, J increments of $\Delta\theta$, and radius R (Fig. 1), a simple explicit finite difference scheme based on the integral forms of the divergence and gradient operators and uniform time step Δt gives the discretization of (8)–(10) as

$$T_{ni,j}^{m+1}=(L_{ni,j1}^m+L_{ni,j2}^m+L_{ni,j3}^m+L_{ni,j4}^m+A_{ni,j1}^m$$
$$+A_{ni,j2}^m)\,\Delta t/[iC(\Delta r)^2\,\Delta\theta\rho_{ni,j}^m],$$
$$i=2,3,...,I; j=1,2,3,...,J\Leftrightarrow 0;$$
$$m=0,1,2,3,...,M; n=0,1,2,3,..., \tag{16}$$

where

$$L_{ni,j1}^m\equiv(\kappa_{ni,j-1}^m+\kappa_{ni,j}^m)(T_{ni,j-1}^m-T_{ni,j}^m)/2i\,\Delta\theta,$$
$$L_{ni,j2}^m\equiv(\kappa_{ni+1,j}^m+\kappa_{ni,j}^m)(T_{ni+1,j}^m-T_{ni,j}^m)(i+\tfrac{1}{2})\,\Delta\theta,$$
$$L_{ni,j3}^m\equiv(\kappa_{ni,j+1}^m+\kappa_{ni,j}^m)(T_{ni,j+1}^m-T_{ni,j}^m)/(-i\,\Delta\theta),$$
$$L_{ni,j4}^m\equiv(\kappa_{ni-1,j}^m+\kappa_{ni,j}^m)(T_{ni-1,j}^m-T_{ni,j}^m)(-i+\tfrac{1}{2})\,\Delta\theta, \tag{17}$$
$$A_{ni,j1}^m\equiv iC\,\Delta\theta(\Delta r)^2\rho_{ni,j}^m T_{ni,j}^m/\Delta t, A_{ni,j2}^m\equiv i\,(\Delta r)^2\Delta\theta Q_{ni,j}^m;$$
$$\kappa_{nI+1,j}^m(-T_{nI-1,j}^m+4T_{nI,j}^m-3T_{nI+1,j}^m)/2\,\Delta r=h(T_{nI+1,j}^m-T_{rI+1,j})$$
$$+s[\beta(T_{nI+1,j}^m)^4-\alpha T_{rI+1,j}^4], j=1,2,3,...,J\Leftrightarrow 0;$$
$$\mathrm{m}=1,2,3,...,M; n=0,1,2,3,...,$$

where $T_{nI+1,j}^m$ can be solved by using the Newton's method;

$$P_{ni,j}^0=T_{ri,j},\quad i=1,2,3,...,I+1;$$
$$j=1,2,3,...,J\Leftrightarrow 0; n=0,1,2,3,.... \tag{18}$$

To satisfy the required stability condition of the above explicit finite difference scheme at the center of the circular cylindrical coordinate, where $i = 1$, the small size of the triangular zones requires Δt to be very small. This difficulty can be overcome by combining the J triangular zones into one single circular zone so that the integration path is the circle centered at $i = 1$ with radius $\Delta r/2$. In this way, Eq. (16) becomes

$$T_{n1}^{m+1}=T_{n1}^m+\Delta tQ_{n1}^m/C\rho_{n1}^m$$
$$+2\,\Delta t[JC(\Delta r)^2\rho_{n1}^m]^{-1}\sum_{j=1}^{J}(\kappa_{n1}^m+\kappa_{n2,j}^m)(T_{n2,j}^m-T_{n1}^m),$$
$$m=0,1,2,3,...,M; n=0,1,2,3,.... \tag{19}$$

Similarly, the finite difference approximations of Eqs. (11)–(13) are

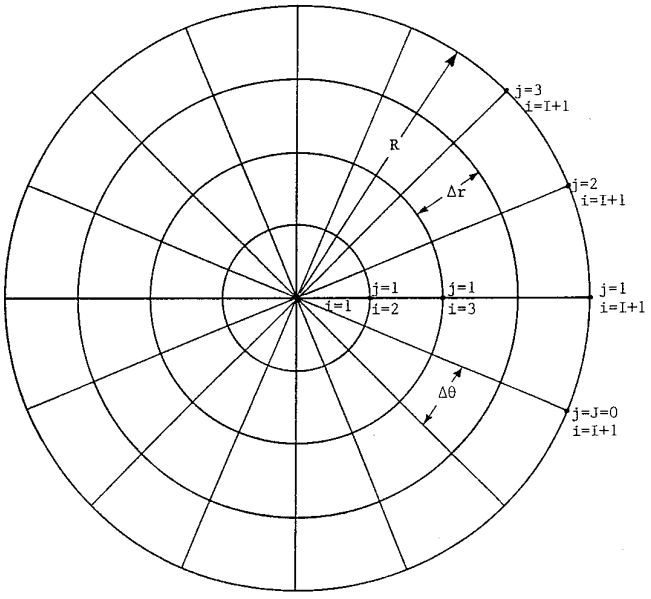

FIG. 1. The circular cyclindrical grid.

$$
\begin{aligned}
&\delta c_{1,ni,j}(T_{ni,j}^{m+1} + T_{ni,j}^{m}) + \delta c_{2,ni,j}[(T_{ni,j}^{m+1})^2 \\
&\quad + (T_{ni,j}^{m})^2] + \delta c_{3,ni,j}[(T_{ni,j}^{m+1})^3 + (T_{ni,j}^{m})^3] \\
&\quad = [i(\Delta r)^2\,\Delta\theta]^{-1}\{2M_{ni,j}^{m+1/2} + 2R_{ni,j}^{m+1/2} \\
&\quad - [\delta L_{ni,j1}^{m+1} + \delta L_{ni,j2}^{m+1} + \delta L_{ni,j3}^{m+1} + \delta L_{ni,j4}^{m+1} \\
&\quad + \delta N_{ni,j1}^{m+1} + \delta N_{ni,j2}^{m+1} + \delta N_{ni,j3}^{m+1} + \delta N_{ni,j4}^{m+1} \\
&\quad + \delta L_{ni,j1}^{m} + \delta L_{ni,j2}^{m} + \delta L_{ni,j3}^{m} + \delta L_{ni,j4}^{m} \\
&\quad + \delta N_{ni,j1}^{m} + \delta N_{ni,j2}^{m} + \delta N_{ni,j3}^{m} + \delta N_{ni,j4}^{m}]\}, \\
&\quad i = 2, 3, ..., I; j = 1, 2, 3, ..., J \Leftrightarrow 0; \\
&\quad m = 0, 1, 2, ..., M; n = 0, 1, 2, 3, ...,
\end{aligned}
\tag{20}
$$

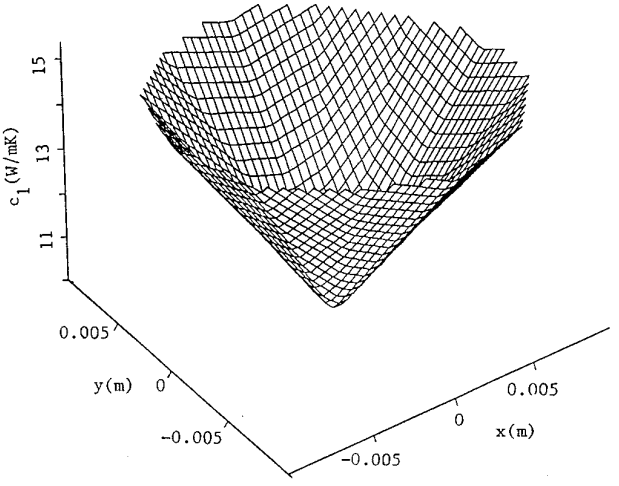

FIG. 3. Computed values of $c_1(\mathbf{x})$ for Example 1.

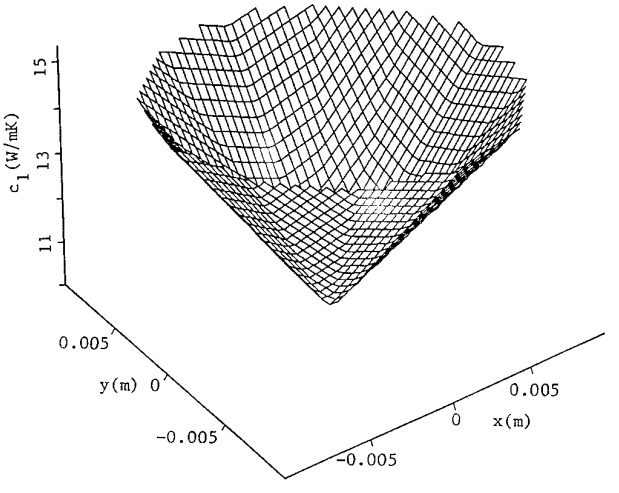

FIG. 4. Exact values of $c_1(\mathbf{x})$ for Example 1.

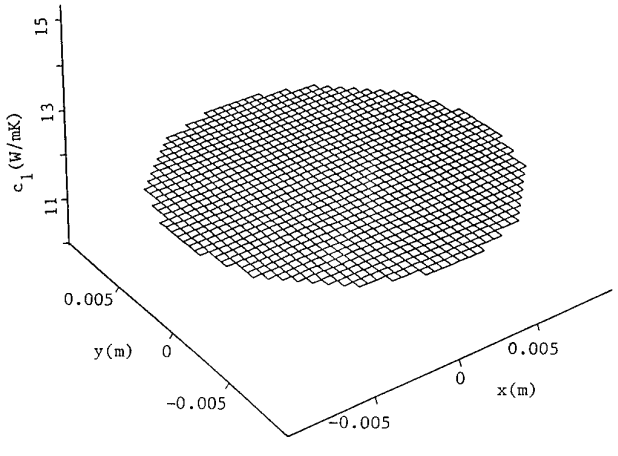

FIG. 2. Initial guess of $c_1(\mathbf{x})$ for Example 1.

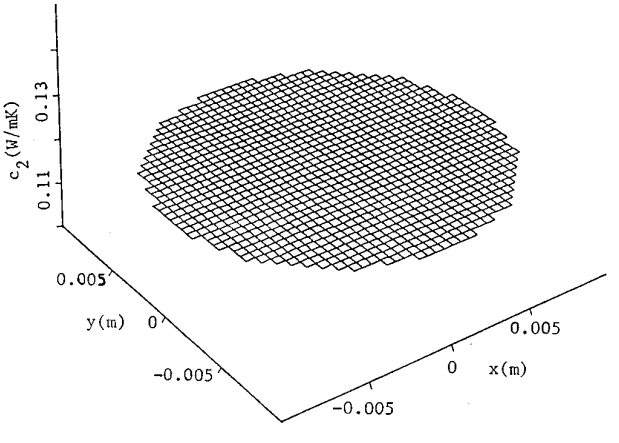

FIG. 5. Initial guess of $c_2(\mathbf{x})$ for Example 1.

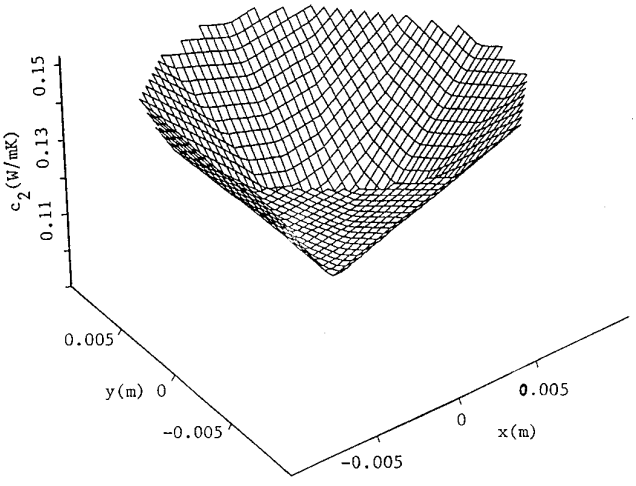

FIG. 6. Computed values of $c_2(\mathbf{x})$ for Example 1.

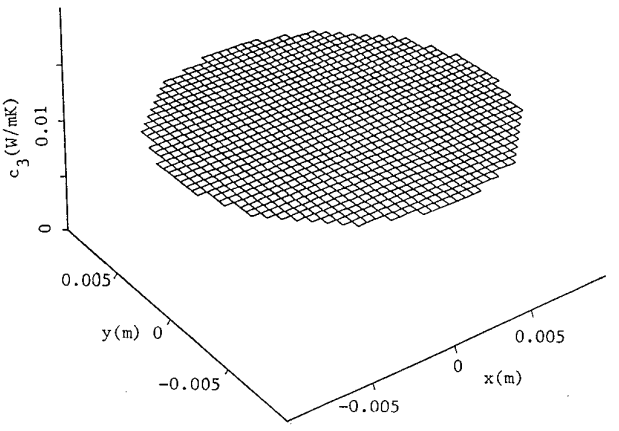

FIG. 8. Initial guess of $c_3(\mathbf{x})$ for Example 1.

where $\delta L^m_{ni,jl}$, $l = 1, 2, 3, 4$, equals $L^m_{ni,jl}$'s with $T^m_{ni,j}$'s being replaced by $\delta T^m_{ni,j}$'s,

$$M^{m+1/2}_{ni,j} \equiv -[i(\Delta r)^2\,\Delta\theta/4][(D^{m+1}_{ni,j} + D^m_{ni,j})(\delta T^{m+1}_{ni,j} + \delta T^m_{ni,j})],$$

$$R^{m+1/2}_{ni,j} \equiv -i(\Delta r)^2\,\Delta\theta(2\,\Delta t)^{-1}[C(\rho^{m+1}_{ni,j} + \rho^m_{ni,j})(\delta T^{m+1}_{ni,j} - \delta T^m_{ni,j}) + (V^{m+1}_{ni,j}\delta T^{m+1}_{ni,j} + V^m_{ni,j}\delta T^m_{ni,j})(T^{m+1}_{ni,j} - T^m_{ni,j})],$$

$$\delta N^m_{ni,j1} \equiv [(U^m_{ni,j-1} + U^m_{ni,j})(T^m_{ni,j-1} - T^m_{ni,j})(\delta T^m_{ni,j-1} + \delta T^m_{ni,j})]/4i\,\Delta\theta,$$

$$\delta N^m_{ni,j2} \equiv [(U^m_{ni+1,j} + U^m_{ni,j})(T^m_{ni+1,j} - T^m_{ni,j})(\delta T^m_{ni+1,j} + \delta T^m_{ni,j})](i + \tfrac{1}{2})\,\Delta\theta/4,$$

$$\delta N^m_{ni,j3} \equiv -[(U^m_{ni,j+1} + U^m_{ni,j})(T^m_{ni,j+1} - T^m_{ni,j})(\delta T^m_{ni,j+1} + \delta T^m_{ni,j})]/4i\,\Delta\theta,$$

$$\delta N^m_{ni,j4} \equiv -[(U^m_{ni-1,j} + U^m_{ni,j})(T^m_{ni-1,j} - T^m_{ni,j})(\delta T^m_{ni-1,j} + \delta T^m_{ni,j})](i - \tfrac{1}{2})\,\Delta\theta/4,$$

$$D^m_{ni,j} \equiv c_{1,ni,j} + 2c_{2,ni,j}T^m_{ni,j} + 3c_{3,ni,j}(T^m_{ni,j})^2,$$

$$U^m_{ni,j} \equiv (\partial\kappa_n/\partial T_n)^m_{i,j}, \quad \text{and} \quad V^m_{ni,j} \equiv C(\partial\rho_n/\partial T_n)^m_{i,j};$$

$$-\kappa^m_{nI+1,j}(\delta T^m_{nI-1,j} - 4\delta T^m_{nI,j} + 3\delta T^m_{nI+1,j})$$

$$= \{2\,\Delta r[h + 4s\beta(\delta T^m_{nI+1,j})^3] + U^m_{nI+1,j}(T^m_{nI-1,j} - 4T^m_{nI,j} + T^m_{nI+1,j})\}\delta T^m_{nI+1,j},$$

$$j = 1, 2, 3, ..., J \Leftrightarrow 0;\ m = 1, 2, 3, ..., M;$$

$$n = 0, 1, 2, 3, ...; \tag{21}$$

$$\delta T^0_{ni,j} = 0, \quad i = 1, 2, 3, ..., I + 1;$$

$$j = 1, 2, 3, ..., J \Leftrightarrow 0;\ n = 0, 1, 2, 3, ... \tag{22}$$

Equations (20)–(22) can be written in the matrix form,

$$\mathbf{a}^{m,m+1}_n \cdot \delta\mathbf{T}^{m+1}_n + \mathbf{b}^{m,m+1}_n \cdot \delta\mathbf{T}^m_n = \mathbf{d}^{m,m+1}_n \cdot \delta\mathbf{c}_n, \quad m = 0, 1, 2, 3, ..., M, \tag{23}$$

where $\mathbf{a}^{m,m+1}_n$ and $\mathbf{b}^{m,m+1}_n$ are the known $(IJ + 1) \times (IJ + 1)$ matrices, $\delta\mathbf{T}_n$'s are the unknown $(IJ + 1)$-dimensional vectors, $\mathbf{d}^{m,m+1}_n$ is the known $(IJ + 1) \times 3(IJ + 1)$ matrix, and $\delta\mathbf{c}_n$ is the unknown $3(IJ + 1)$-dimensional vector arranged in the form $(\delta\mathbf{c}_{1,n}, \delta\mathbf{c}_{2,n}, \delta\mathbf{c}_{3,n})^{\mathrm{T}}$.

Upon collecting all of the equations in (23) corresponding to the spatial data points $\mathbf{x}_p$, $p = 1, 2, 3, ..., P$, where

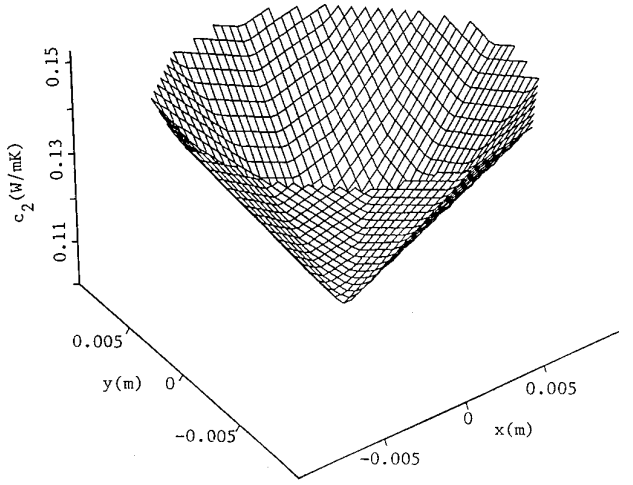

FIG. 7. Exact values of $c_2(\mathbf{x})$ for Example 1.

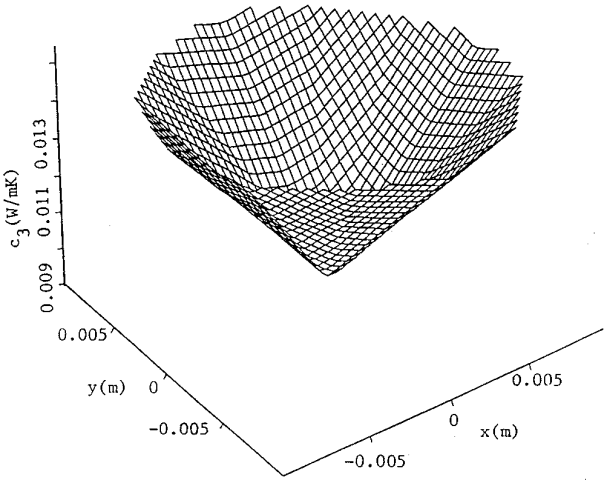

FIG. 9. Computed values of $c_3(\mathbf{x})$ for Example 1.

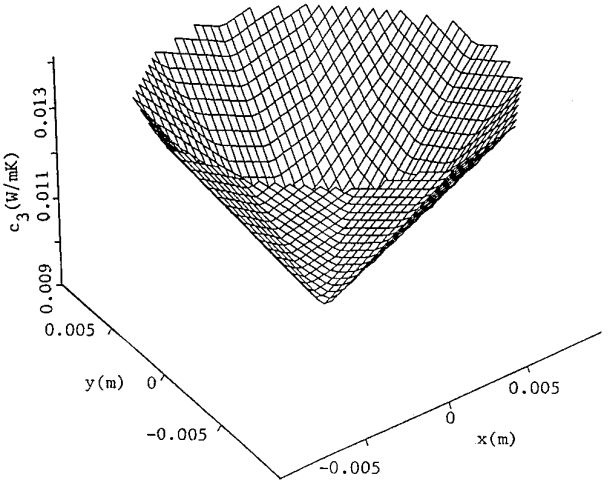

FIG. 10. Exact values of $c_3(\mathbf{x})$ for Example 1.

the surface temperature measurements are performed, and replacing $T^{\upsilon}_{n+1i,j}(\mathbf{x}_p, t_\upsilon)$ by their corresponding measured values $T_S(\mathbf{x}_p, t_\upsilon)$, one obtains a compact linear algebraic system for each υ,

$$\mathbf{D}^{\upsilon}_n \cdot \delta\mathbf{c}_n = \mathbf{S}^{\upsilon}_n, \quad \upsilon = 1, 2, 3, ..., \Upsilon; n = 0, 1, 2, 3, ..., \tag{24}$$

where $\mathbf{D}^{\upsilon}_n$ is the known $P \times 3(IJ + 1)$ full matrix and $\mathbf{S}^{\upsilon}_n$ is the known P-dimensional vector.

To obtain an overdetermined system for $\delta\mathbf{c}_n$, one can choose Υ large enough and cascade Υ of the underdetermined system of (24) into a single system to acquire

$$\mathbf{D}_n \cdot \delta\mathbf{c}_n = \mathbf{S}_n, \quad n = 0, 1, 2, 3, ..., \tag{25}$$

where $\mathbf{D}_n$ is the known $\Upsilon P \times 3(IJ + 1)$ full matrix, $\mathbf{S}_n$ is the known ΥP-dimensional vector, and $\Upsilon P \geq 3(IJ + 1)$.

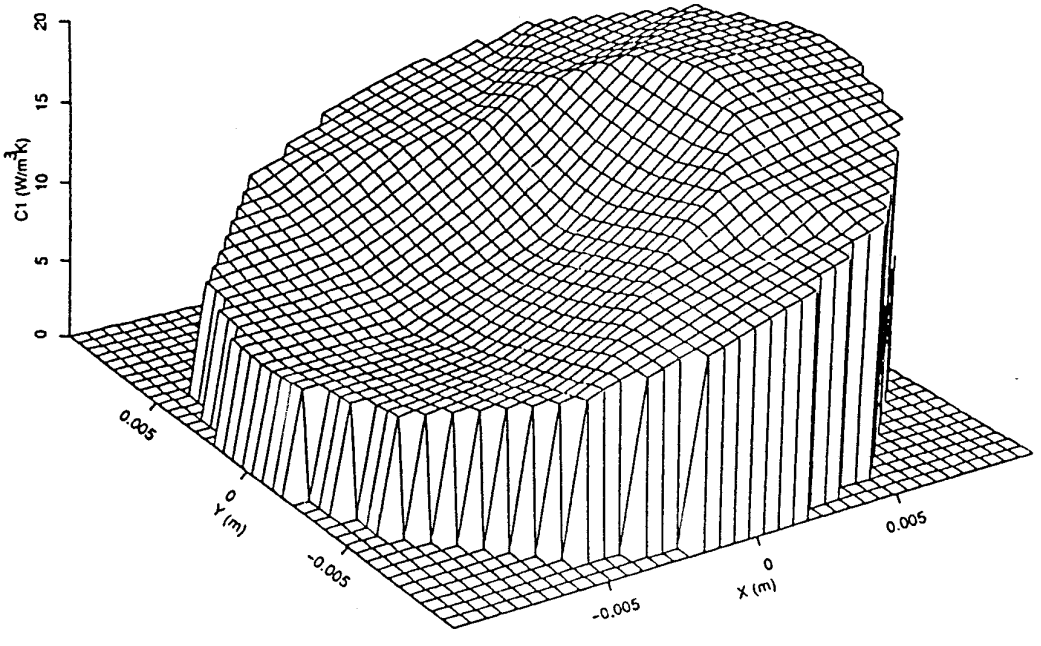

FIG. 11. Computed values of $c_1(\mathbf{x})$ for Example 2.

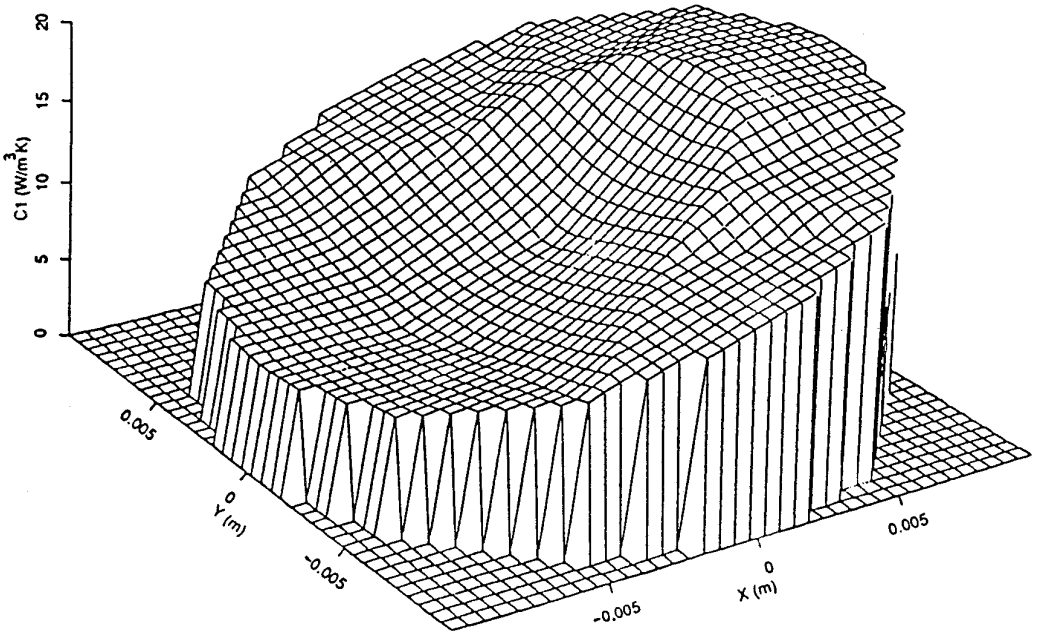

FIG. 12. Exact values of $c_1(\mathbf{x})$ for Example 2.

Unfortunately, $\mathbf{D}_n$ is rectangular and $\mathbf{D}_n^{\mathrm{T}} \cdot \mathbf{D}_n$ is highly ill-conditioned; hence Tikhonov regularization method [19] is used to overcome this difficulty; i.e., instead of solving (25), one solves the regularized system,

$$(\mathbf{D}_n^{\mathrm{T}} \cdot \mathbf{D}_n + \lambda \mathbf{I}) \cdot \delta \mathbf{c}_n = \mathbf{D}_n^{\mathrm{T}} \cdot \mathbf{S}_n, \quad n = 0, 1, 2, 3, ..., \qquad (26)$$

where λ is the regularization parameter.

Here, in essence, each cycle of GPST iteration consists of a direct half-cycle in which Eqs. (16)–(19) are solved and an inverse half-cycle in which Eqs. (26) and (7) are solved. Simple computational complexity analysis, as before, can show that the bottle neck in computation lies mainly in the inverse half-cycle of GPST iteration.

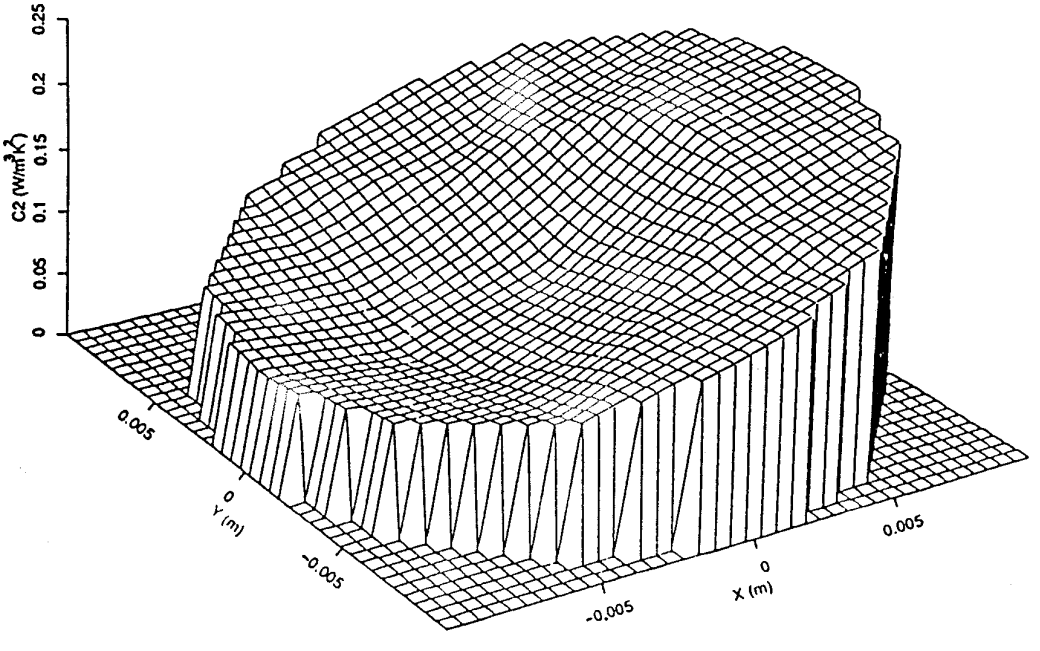

FIG. 13. Computed values of $c_2(\mathbf{x})$ for Example 2.

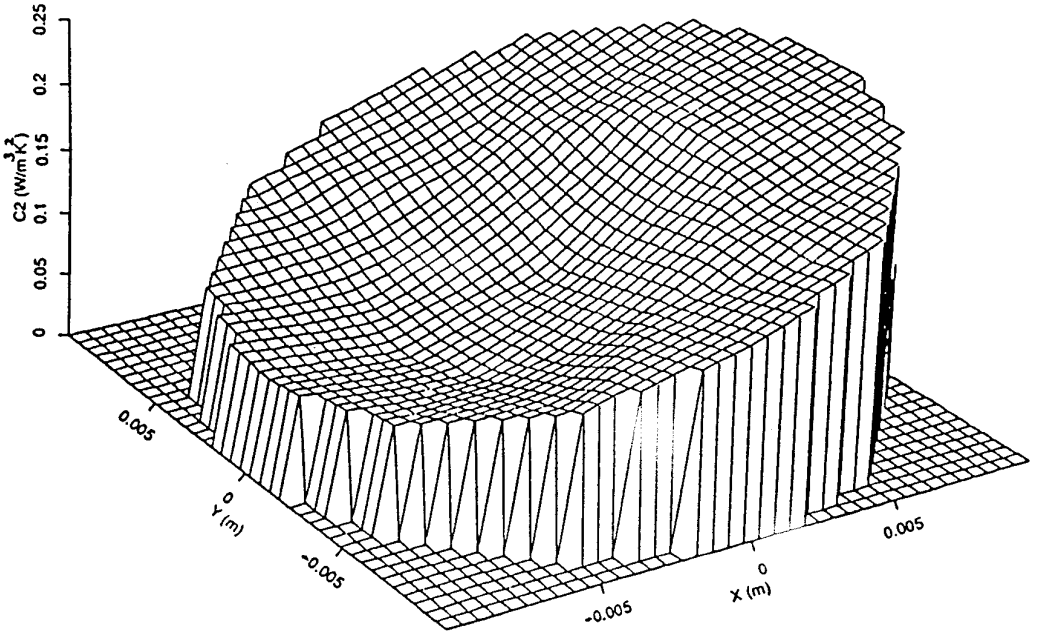

FIG. 14. Exact values of $c_2(\mathbf{x})$ for Example 2.

A MULTILEVEL GRID METHOD

To improve the efficiency and stability of the standard GPST inversion algorithm, a multilevel grid method simpler than that of Chen and Zhang [8] and Chen [9], but similar to that of Zhu and Chen [20] is incorporated into the standard GPST algorithm. Let Γ_0 be the coarsest grid and a sequence of successively finer grids $\Gamma_0 \subset \Gamma_1 \subset \Gamma_2 \subset \cdots \subset \Gamma_F$ be constructed by dividing each zone element of the next coarser grid. Here the multilevel grid method requires that $T_{ni,j}^{m+1}$ of (16)–(19) is solved on Γ_F for all iterations. It also requires $\delta\mathbf{c}_n$ of (26) to be solved on Γ_0

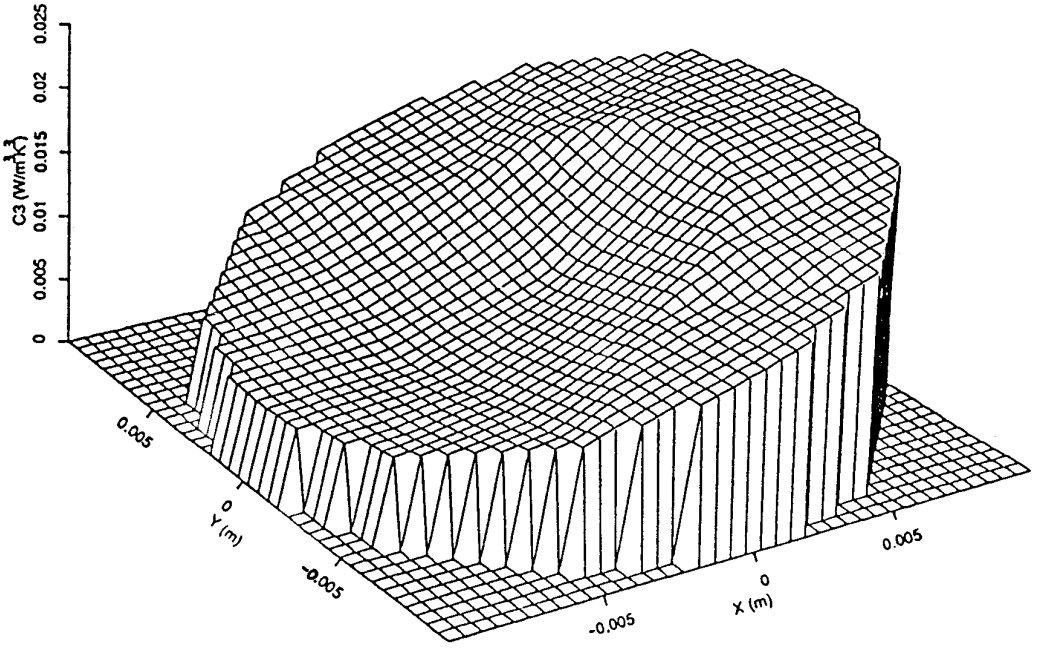

FIG. 15. Computed values of $c_3(\mathbf{x})$ for Example 2.

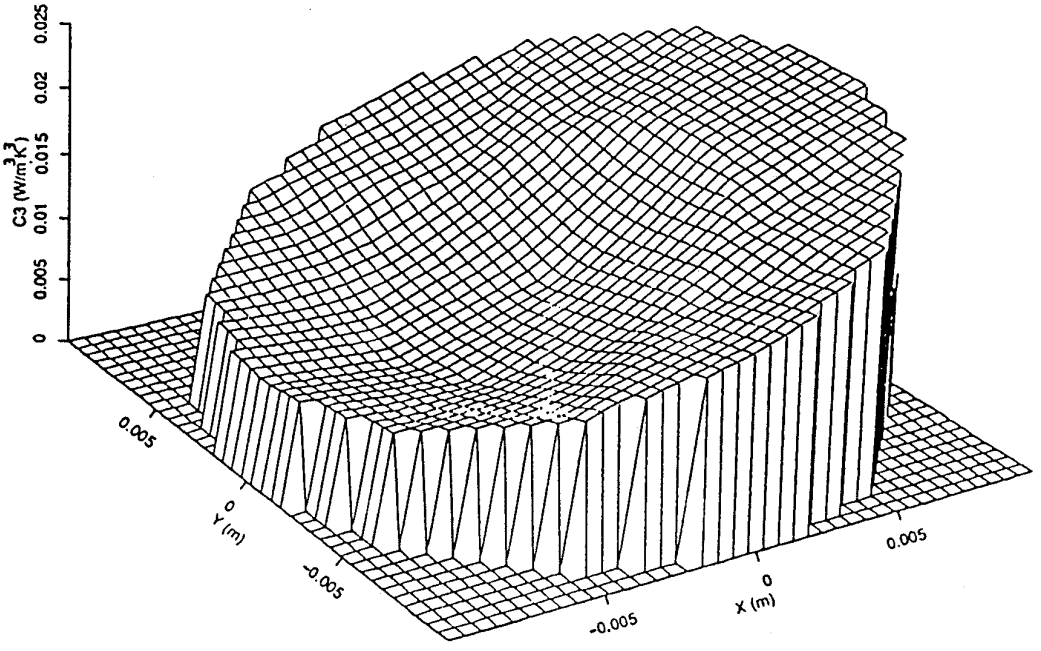

FIG. 16. Exact values of $c_3(\mathbf{x})$ for Example 2.

for the first few iterations; then its numerical values are interpolated into Γ_1 as the initial guess for the next few iterations. Next, the numerical values of $\delta\mathbf{c}_n$ on Γ_1 are interpolated into Γ_2 as the initial guess for the next few iterations. One continues this process until the final numerical values of $\delta\mathbf{c}_n$ are calculated on the finest grid Γ_F. In this way, the number of iterations on Γ_F for solving $\delta\mathbf{c}_n$ is greatly reduced. Since the total computational cost for solving $\delta\mathbf{c}_n$ on all coarser grids is minuscule in comparison with that for one iteration on Γ_F, the efficiency of the standard GPST inversion algorithm is greatly improved. Furthermore, because of the systematic improvement of the initial guesses, the stability is also greatly ameliorated.

PARAMETER-SPACE PARALLELISM

Here the parameter-space parallelism first requires the unknown parameter correction vector $\delta\mathbf{c}_n$ to be decomposed into three subvectors $\delta\mathbf{c}_{1,n}$, $\delta\mathbf{c}_{2,n}$, and $\delta\mathbf{c}_{3,n}$. Then these three subvectors can be obtained independently by solving three uncoupled subsystems,

$$(\mathbf{D}_{l,n}^{\mathrm{T}} \cdot \mathbf{D}_{l,n} + \lambda_l \mathbf{I}) \cdot \delta\mathbf{c}_{l,n} = \mathbf{D}_{l,n}^{\mathrm{T}} \cdot \mathbf{S}_n, \qquad l = 1, 2, 3; n = 0, 1, 2, 3, ..., \tag{27}$$

where $\mathbf{D}_n \equiv (\mathbf{D}_{1,n}, \mathbf{D}_{2,n}, \mathbf{D}_{3,n})$ and $\mathbf{D}_{l,n}^{\mathrm{T}} \cdot \mathbf{D}_{l,n}$'s are symmetric $(IJ + 1)$-dimensional matrices.

It is clear that every subsystem of (27) can be solved separately, either on an individual cluster of processors in parallel or on a single processor sequentially. Moreover, this parallelism can be incorporated directly into the multilevel grid method with great ease. The efficiency is greatly improved here because each subsystem is much smaller than the original system.

NUMERICAL SIMULATIONS

In order to test the feasibility and capability of this new GPST inversion algorithm without real measurement data, the following numerical simulation procedure is carried out. First, a set $\{c_l^*(\mathbf{x})\}$, $l = 1, 2, 3$, is chosen as the supposedly correct values of $\{c_l(\mathbf{x})\}$, $l = 1, 2, 3$. Then Eqs. (2)–(5) are solved to get the supposedly measured surface temperature $T_S(\mathbf{x}, t)$. Next, these computer-generated data are used in the inversion algorithm to obtain a set of approximate parameters $\{c_{l,F}(\mathbf{x})\}$, $l = 1, 2, 3$. The magnitude of the norms $\|c_l^* - c_{l,F}\|$, $l = 1, 2, 3$, can be used as a criterion for evaluating the performance of this improved GPST inversion algorithm. Our tests have shown that even with a random error of 1% in the input data the results are still very good.

Many examples are used in our numerical simulations and it is found that this new GPST inversion algorithm produces very good results for all of them. Due to the large amount of graphs needed to present the numerical results of just one example, only the results of two typical examples with the same initial guesses are presented here in Figs. 2–10 (Example 1) and Figs. 11–16 (Example 2). For easy estimation of errors, a typical plot (Example 2)

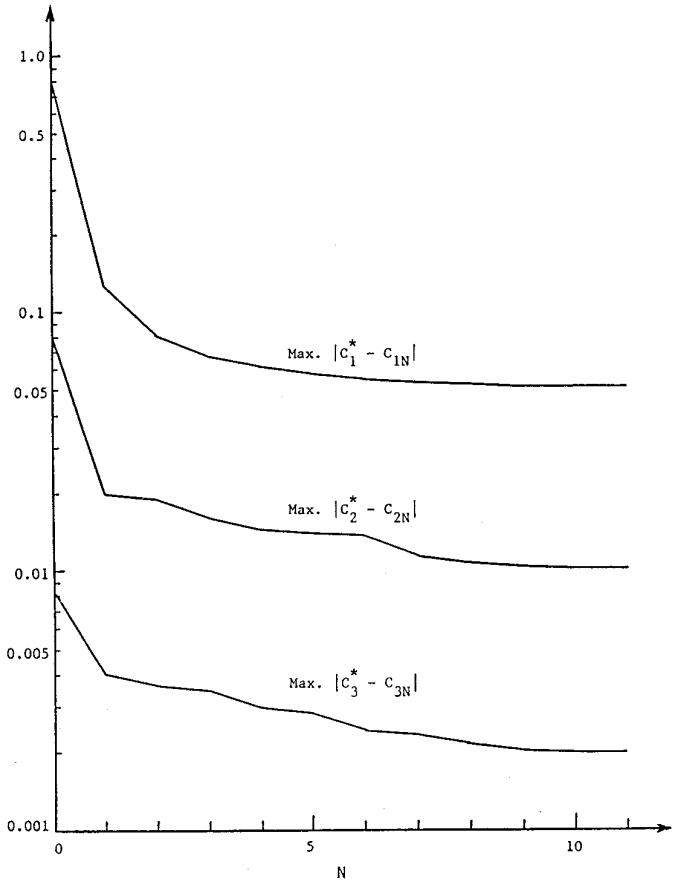

FIG. 17. Plots of Max$|c_l^* - c_{l,n}|$ vs. n, $l = 1, 2, 3$, for Example 2, with units W/m^{3}K, W/m^{3}K^2, and W/m^{3}K^3, respectively.

of Max$|c_l^* - c_{l,n}|$, $l = 1, 2, 3$, as functions of "n" is given in Fig. 17.

For these two examples, a typical ceramic sample with $\kappa(\mathbf{x}, t) = a_0(\mathbf{x}) + a_1(\mathbf{x})T + a_2(\mathbf{x})T^2 + a_3(\mathbf{x})T^3$ and $C\rho(\mathbf{x}, t) = b_0(\mathbf{x}) + b_1(\mathbf{x})T + b_2(\mathbf{x})T^2 + b_3(\mathbf{x})T^3$ is considered. For Example 1, $a_0 = 0.06(1 + r/2R)$ W/mK and $b_0 = 2092(1 + r/2R)$ kJ/m^{3}K and for Example 2, $a_0 = 0.06$ W/mK and $b_0 = 2092$ kJ/m^{3}K. For both examples, $a_1 = 0.1a_0$ 1/K, $a_2 = 0.01a_0$ 1/K^2, $a_3 = 0.001a_0$ 1/K^3, $b_1 = 0.1b_0$ 1/K, $b_2 = 0.01b_0$ 1/K^2, $b_3 = 0.001b_0$ 1/K^3, $h = 0.95$ W/m^{2}K, $s = 5.6696 \times 10^{-9}$ W/m^{2}K^4, $\alpha = \beta = 0.92$, $\Delta t = 1$ s, the finest (third) level of grid $\Delta r = 0.005$ m, $\Delta\theta = \pi/8$, and there are eight data points uniformly distributed at $i = I + 1$. Moreover, the same regularization parameters, $\lambda_1 = 10^{-11}$, $\lambda_2 = 10^{-8}$, and $\lambda_3 = 10^{-6}$, are used in both examples.

On a single SUN SPARC II workstation, approximately 7.5 min of computer time is needed for each complete inversion. Since we are not able to obtain access to a multiprocessor computer, the estimated computer time would be approximately less than 3 min on a cluster of three similar workstations in parallel. On the other hand, when the standard GPST is used for the same inverse problem, 350 min of computer time is needed on the same workstation. Hence the efficiency of the standard GPST inversion algorithm is improved at least by a factor of 100 on a multiprocessor computer and this is quite remarkable.

CONCLUSIONS

The capacity of this GPST inversion algorithm with the multilevel grid and the parameter-space parallelism for solving three-parameter 2D inverse source problem of a nonlinear diffusion equation has been clearly demonstrated in our numerical simulations. The excellent performance for this simple prototype of inversion code has definitely encouraged us to develop a similar 3D code with an irregular spherical grid system for solving the "real" inverse source problem of the nonlinear diffusion equation in the microwave heating.

REFERENCES

1. R. L. Beatty, W. H. Sutton, and M. F. Iskander, *Microwave Processing of Materials III,* MRS Symp. Proc., Vol. 269, 1992.
2. J. V. Beck *et al. Inverse Heat Conduction: Ill-Posed Problems* (Wiley, New York, 1985).
3. J. R. Cannon and P. DuChateau, *J. Heat Transfer* **100,** 503 (1978).
4. S. Chang and W. Yeh, *Water Resource Res.* **12,** 365 (1976).
5. Y. M. Chen, *Computers & Structures* **30,** 821 (1988).
6. Y. M. Chen and J. Q. Liu, *J. Comput. Phys.* **43,** 315 (1981).
7. Y. M. Chen and J. Q. Liu, *J. Comput. Phys.* **53,** 429 (1984).
8. Y. M. Chen and F. G. Zhang, *Appl. Numer. Math.* **6,** 431 (1989/1990).
9. Y. M. Chen, in *Geophysical Inversion* (J. Bee Bednar, L. R. Lines, R. H. Stolt, and A. B. Weglein, Eds.) SIAM, Philadelphia, 1992), p. 277.
10. E. Hensel, *Inverse Theory and Applications of Engineers* (Prentice–Hall, Englewood Cliffs, NJ, 1991).
11. C. Kravaris and J. H. Seinfeld, *SIAM J. Control & Optim.* **24,** 522 (1986).
12. J. Q. Liu and Y. M. Chen, *SIAM J. Sci. Comput.* **5** 255 (1984).
13. X. Y. Liu and Y. M. Chen, *SIAM J. Sci. Comput.* **8** 436 (1987).
14. G. Ponzini, G. Crosta and M. Giudici, *Geophysics* **54** 643 (1989).
15. W. M. Rohsenow *et al., Handbook of Heat Transfer* (McGraw–Hill, New York, 1973).
16. W. B. Snyder Jr., W. H. Sutton, and M. F. Iskander, *Microwave Processing of Materials II,* MRS Symp. Proc., Vol. 189, 1991.
17. W. H. Sutton, *Am. Ceramic Soc. Bul.* **68** 376 (1989).
18. W. H. Sutton, M. H. Brooks, and I. J. Chabinsky, *Microwave Processing of Materials,* MRS Symp. Proc., Vol. 124, 1988.
19. A. N. Tikhonov and V. Y. Arsenin, *Solutions of Ill-Posed Problems* (Wiley, New York, 1977).
20. J. Zhu and Y. M. Chen, *Appl. Numer. Math.* **10,** 159 (1992).